PHYSICAL REVIEW D **90,** 122008 (2014)

Time evolution of parametric instability in large-scale gravitational-wave interferometers

Stefan L. Danilishin,[1,*] Sergey P. Vyatchanin,[2] David G. Blair,[1] Ju Li,[1] and Chunnong Zhao[1]

[1]*School of Physics, UWA, 35 Stirling Highway, Crawley, Western Australia 6009, Australia*

[2]*Faculty of Physics, M.V. Lomonosov Moscow State University, Moscow 119991, Russia*

(Received 25 September 2014; published 29 December 2014)

We present a study of three-mode parametric instability in large-scale gravitational-wave detectors. Previous work used a linearized model to study the onset of instability. This paper presents a nonlinear study of this phenomenon, which shows that the initial stage of an exponential rise of the amplitudes of a higher-order optical mode and the mechanical internal mode of the mirror is followed by a saturation phase, in which all three participating modes reach a new equilibrium state with constant oscillation amplitudes. Results suggest that stable operation of interferometers may be possible in the presence of such instabilities, thereby simplifying the task of suppression.

DOI: 10.1103/PhysRevD.90.122008 PACS numbers: 04.80.Nn, 42.65.Es, 42.65.Yj, 95.55.Ym

I. INTRODUCTION

Three-mode parametric instability in large-scale, high-optical-power gravitational-wave (GW) detectors was predicted by Braginsky *et al.* in 2001 [1]. All subsequent analyses [2–5] relied on the model prediction, where amplitudes of certain acoustic modes of the interferometer mirrors would grow exponentially once an instability threshold of input laser power is reached. It was generally considered that the exponential growth would eventually render the whole setup unstable and cause an interferometer to lose lock.

This prognosis, however, relied on a linearized approximation of the three-mode optomechanical interaction that is valid only for small amplitudes of acoustic and Stokes modes. For larger values, it is intuitively obvious that nonlinearity should ultimately modify this growth. If the optical configuration can be maintained one would expect that the acoustic and higher-order optical oscillations should saturate. Knowing the amplitudes of such saturation effects as well as their time scale is of crucial importance for the operation of the real detectors now being implemented.

It is hard to overestimate the significance of rigorous analysis of this phenomenon in large-scale gravitational-wave interferometers. Second-generation detectors, such as Advanced LIGO [6,7] are at the latest stages of construction and testing. These instruments are planned to have up to ~800 kW of circulating laser power in the arms. As demonstrated in [3–5,8,9], the chance of three-mode parametric instability at such a high level of power is very high. Similarly, other advanced detectors, Advanced Virgo [10], KAGRA [11], and GEO-HF [12], might also be susceptible to this effect, though with different probabilities (see Ref. [2] for details).

Therefore, knowledge of the temporal dynamics and the values of final amplitudes that the three participating modes reach at the saturation stage allows us to design a feedback control system to suppress this instability before it develops. Several methods of mitigating this phenomenon have been developed that can benefit from this information: (i) Varying the mirrors' radii of curvature by heating [13–15]; (ii) decreasing the Q factor of the acoustic modes [14,16,17]; and (iii) introducing additional damping to acoustic modes via electrostatic feedback [18].

In this paper, we present a full nonlinear treatment of this problem for large-scale gravitational-wave interferometers. A similar approach has been used by Polyakov and Vyatchanin in [19] to study the precursors of parametric instability (PI) in the regime of input powers close to the PI threshold. In this paper, we expand and generalize their treatment to arbitrary input power levels and investigate the time evolution of the amplitudes of the Stokes and pump optical modes as well as of the acoustic mode. It is noteworthy that the set of dynamical equations in this work is similar to those in [19], yet we prove that the smallness requirement of the mechanical mode amplitude (allegedly, it has to be smaller than the linewidth of the optical modes) stated therein is not necessary, and this model is valid for arbitrarily large acoustic amplitudes.

In addition, a similar effect has been observed and analyzed in small-scale whispering-gallery-mode optical resonators used to create stable-radio-frequency optomechanical oscillators [20,21]. Recently, the saturation of unstable oscillations has been observed at the University of Western Australia (UWA) and in the Laboratoire Kastler Brossel in tabletop optomechanical experiments using a high-finesse Fabry-Pérot cavity with a silicon nitride membrane acting as the acoustic resonator test mass [22]. In that paper, we derived a similar model to back the experimental results. In this paper, we focus on a different physical system that comprises massive freely

*stefan.danilishin@ligo.org

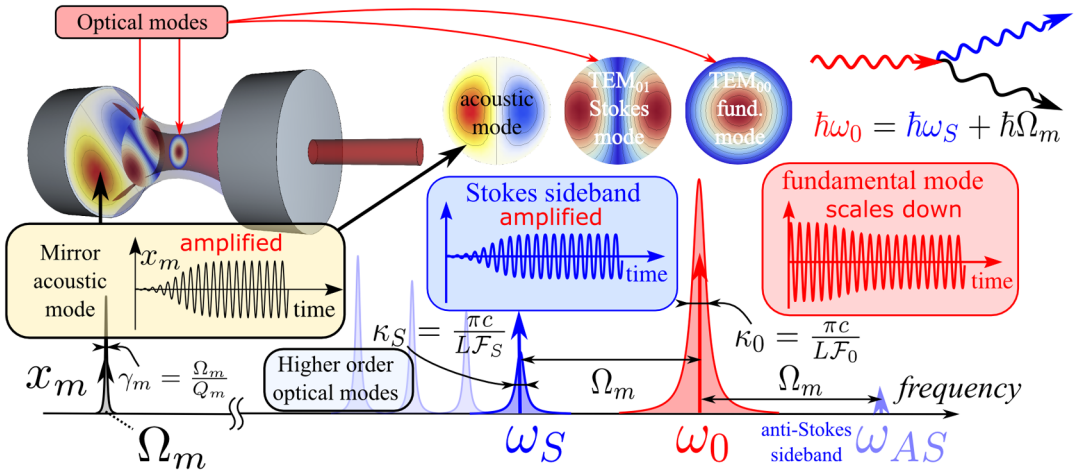

FIG. 1 (color online). Schematic of the three-mode interaction that gives rise to parametric instability in optomechanical systems: (i) Acoustic modes of the mirror, excited by thermal fluctuations, create motional sidebands of the pump mode carrier frequency offset by acoustic frequency Ω_m; (ii) the lower-frequency Stokes sideband is enhanced by a higher-order optical cavity mode—a beat note between this and the fundamental pump mode creates a radiation pressure force at the acoustic frequency Ω_m; (iii) this leads to a growth of the acoustic oscillation amplitude, which, in turn, increases the amplitude of the Stokes sideband, thereby raising radiation pressure force amplitude and closing the instability feedback loop. The strength of the three-mode optomechanical interaction, and, therefore, the chance of instability development, depends on the following three factors: (i) The extent to which the spatial distributions of all three participating modes overlap, characterized by overlapping factor Λ_{0S}, defined in Eq. (6); (ii) the accuracy of three-mode frequency tuning—i.e., detuning must be smaller than the larger of optical modes bandwidth, $\Delta_m = \omega_0 - \omega_S - \Omega_m \ll \max[\kappa_0, \kappa_S]$; and (iii) the energy loss rates in all three modes, which need to be lower than the rate of power transfer between the modes, which itself is characterized by the coupling strength G_{0S}. These three conditions yield the definition of parametric gain, $\mathcal{R}_0$, given in Eq. (10), and the condition for PI given by Eq. (11).

suspended Fabry-Pérot cavities that interact with a high-power optical field circulating inside. We also analyze the three-mode parametric instability phenomenon in more detail and with greater generality.

The physics of three-mode parametric instability is illustrated in Fig. 1. We consider a Fabry-Pérot interferometer pumped at a laser frequency ω_p close to the resonance frequency, ω_0, of one of the fundamental modes [23]. Ultrasonic vibrations of the mirrors with frequency Ω_m cause intracavity light to scatter into two motional sidebands: A Stokes one, with frequency $\omega_S = \omega_0 - \Omega_m$, and an anti-Stokes one, with frequency $\omega_{\mathrm{AS}} = \omega_0 + \Omega_m$. As the fundamental mode linewidth κ_0 is normally much smaller than Ω_m, the amplitude of motional sidebands is normally not enhanced by the cavity. This is not so, however, if the sideband frequency coincides with one of the higher-order optical mode (HOM) frequencies. Such modes exist in any Fabry-Peŕot cavity and densely populate the free spectral range between the fundamental modes (see Sec. 3.3 of [23]). If the transverse spatial profile of such a HOM matches the profile of an acoustic vibration, the photons scattered into this mode from the fundamental mode build up, thereby channeling part of the optical power circulating in the fundamental mode to the HOM.

The beat note of the fundamental mode and the HOM creates a near-resonant radiation pressure force on the mirror at the frequency of the acoustic mode, Ω_m. Now there are two possibilities to consider. If the HOM frequency coincides (approximately) with the anti-Stokes sideband frequency, ω_{AS}, the radiation pressure force will be applied out of phase with the acoustic vibrations, thereby damping them [24]. This effect is analogous to radiation pressure cooling [25–29], where the scattered Stokes photon energy is a sum of the fundamental mode energy and the acoustic mode phonon energy, i.e., $\hbar\omega_{\mathrm{AS}} = \hbar\omega_0 + \hbar\Omega_m$.

The instability we are studying in this paper, on the contrary, occurs when the HOM frequency matches the Stokes sideband frequency ω_S: $\hbar\omega_S = \hbar\omega_0 - \hbar\Omega_m$. To distinguish this HOM from others we will call it hereafter a Stokes mode. In this case, the radiation pressure force of the beat note is in phase with the acoustic oscillations, leading to amplification. This, in turn, makes amplitude of the Stokes sideband larger, thereby increasing the amplitude of the radiation pressure force. Therefore, the loop closes and the instability breaks out. An illuminating description of this process in terms of feedback control theory can be found in the work of Evans *et al.* [5].

The picture above gives no account for natural decay of the Stokes mode and acoustic oscillations due to loss, characterized by Stokes mode linewidth κ_S and acoustic mode decay rate γ_m. These loss mechanisms counterbalance the instability, and for circulating power below a certain threshold (see below), there is no instability.

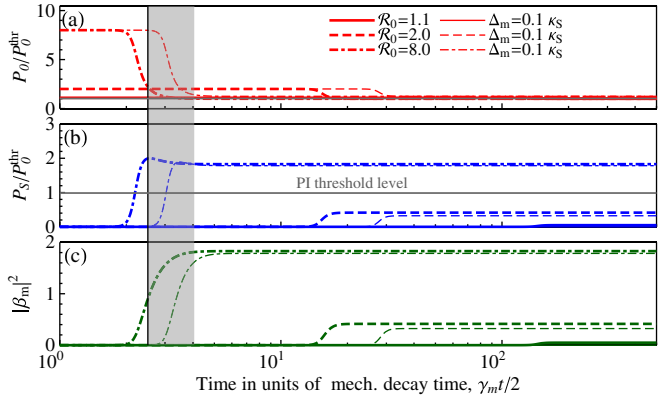

FIG. 2 (color online). Temporal behavior of three interacting modes for different values of PI gain $\mathcal{R}_0$. Thin lines show temporal dynamics in the detuned case with frequency mismatch $\Delta_m = 0.1\kappa_S$. The amplitudes of optical modes are normalized by the maximal value of optical power circulating in the fundamental mode which corresponds to PI gain value of $\mathcal{R}_0 = 8$. The acoustic mode amplitude is scaled by a displacement amplitude b_0 necessary to shift the Stokes mode frequency by one-half linewidth, as per definition in Eq. (7). The greyed-out area and thin vertical line (indicating the maximum of the Stokes mode curve for $\mathcal{R}_0 = 8$) marks the time interval where inverse scattering process, $\hbar\omega_S + \hbar\Omega_m \to \hbar\omega_0$, intensifies in the system with PI gain larger than that defined by condition (20).

However, as soon as the power circulating in the fundamental mode reaches this threshold value, the three-mode instability sets in. A very similar process happens in optical parametric oscillators, where above a certain threshold of pump power, in the presence of strong Kerr nonlinearity of the medium, pump photons scatter into pairs of idler and signal photons [30].

This process resembles a relief valve operation, when above a certain pressure the valve opens and redirects the excess fluid flow into a reserve pipe, keeping the main pipe pressure constant. Similarly, above the instability threshold, all the excess optical power is redirected from the fundamental mode to the Stokes mode and the acoustic mode oscillations. New steady-state amplitudes of all three participating modes are reached when the balance of power is restored in the system, meaning that the amount of power pumped into the system matches the sum power leaving it through the three decay channels, characterized by the decay rates of the two optical modes, κ_0 and κ_S, and a mechanical decay rate, γ_m.

In this paper, we present a nonlinear theory of the three-mode parametric instability in large-scale gravitational-wave interferometers with free suspended mirrors. We derive and solve equations of motion for the amplitudes of three participating modes and obtain their temporal dynamics. To characterize the behavior of unstable modes, we calculate values of new steady-state amplitudes and give an estimate of the instability development time scale.

II. MODEL

A. Hamiltonian of three-mode interaction

To represent parametric instability in large-scale GW interferometers, we use a simple model of a Fabry-Pérot cavity with resonance frequency ω_0 pumped with a laser, having frequency ω_p and power $P_{\rm in}$. Below, we choose to adhere to a Hamiltonian description of the system under study, in contrast with the original work of Braginsky *et al.* [1] where a completely equivalent Lagrangian approach has been used to derive equations of motion of interacting modes. It is worth emphasizing that our analysis below is purely classical and no quantum effects are taken into account in this manuscript. Nevertheless, the choice of a Hamiltonian classical description allows for an easy expansion of this model to a quantum one. As a matter of fact, it has been done recently in the work that predicted a new source of quantum radiation pressure noise in gravitational-wave interferometers originating from the three-mode optomechanical interaction [31].

If we assume intracavity light to be linearly polarized and to propagate along the cavity optical axis z, its electric and magnetic field strain components can be represented, in terms of expansion over cavity modes, as

$$E(t,\vec{r}_\perp,z) = \sum_J \sqrt{\frac{\hbar\omega_J}{\epsilon_0 V}} f_J(\vec{r}_\perp)\sin(\omega_J z/c) \times [a_J(t) + a_J^\dagger(t)], \tag{1a}$$

$$H(t,\vec{r}_\perp,z) = -i\sum_J \sqrt{\frac{\hbar\omega_J}{\mu_0 V}} f_J(\vec{r}_\perp)\cos(\omega_J z/c) \times [a_J(t) - a_J^\dagger(t)], \tag{1b}$$

where $\hbar$, c, ϵ_0, and μ_0 stand for Planck's constant, the speed of light, and vacuum permittivity and permeability, respectively; $V = L\mathcal{A}$ is the volume of the cavity of length L occupied by a light beam with cross-section area $\mathcal{A}$; $f_J(\vec{r}_\perp)$ is the Jth mode spatial distributions in the direction perpendicular to the propagation direction, and a_J denotes dimensionless complex amplitudes of the mode with frequency ω_J normalized so that $n_J = a_J^\dagger a_J = |a_J|^2$ represents the number of photons in the corresponding mode. The acoustic mode of the mirror can be described in terms of surface deflection component along the z-axis: $\zeta(\vec{r}_\perp,t) = x_{\rm z.p} u_z(\vec{r}_\perp)[b_m(t) + b_m^\dagger(t)]$ with $u_z(\vec{r}_\perp)$ being the transverse mode spatial shape and $x_{\rm z.p.} = \sqrt{\hbar/(2m\Omega_m)}$ is the amplitude of the ground state oscillations for an oscillator with effective mass m and eigenfrequency Ω_m.

Since parametric instability occurs only for the modes that satisfy a certain matching condition $\omega_0 = \omega_S + \Omega_m + \Delta_m$ (detuning should be smaller than the larger of the

Stokes or fundamental mode linewidth, $\Delta_m \ll \max[\kappa_S, \kappa_0]$), we can limit our consideration to those three modes (with $J = 0,\ S$). The Hamiltonian for this three-mode interacting system reads

$$\mathcal{H} = \mathcal{H}_m - \frac{1}{2}\int_{\mathcal{A}} d\vec{r}_\perp (L+\zeta)[\epsilon_0(E_0+E_S)^2 + \mu_0(H_0+H_S)^2], \tag{2}$$

with $\mathcal{H}_m = \hbar\Omega_m b_m^\dagger b_m$ and the last term describing the well-known optomechanical interaction when radiation pressure force ($\propto$ light intensity) acts on a mechanical degree of freedom. After integration over transverse coordinates, $\vec{r}_\perp$, one can rewrite it in a more familiar representation,

$$\mathcal{H} = \mathcal{H}_0 + \mathcal{H}_S + \mathcal{H}_m + \mathcal{H}_{0S} + \mathcal{H}_{00} + \mathcal{H}_{SS} + \mathcal{H}_{\text{drive}}, \tag{3}$$

where free evolution Hamiltonians for optical modes can be written as $\mathcal{H}_J = \hbar\omega_J a_J^\dagger a_J$ $(J = 0,\ S)$, $\mathcal{H}_m = \hbar\Omega_m b_m^\dagger b_m$, and optomechanical interaction terms read

$$\mathcal{H}_{0S} = -\hbar G_{0S}(b_m + b_m^\dagger)(a_0 + a_0^\dagger)(a_S + a_S^\dagger), \tag{4a}$$

$$\mathcal{H}_{00} = -\hbar G_{00}(b_m + b_m^\dagger)a_0^\dagger a_0, \tag{4b}$$

$$\mathcal{H}_{SS} = -\hbar G_{SS}(b_m + b_m^\dagger)a_S^\dagger a_S \tag{4c}$$

with optomechanical coupling strengths defined as

$$G_{IJ} = x_{\text{z.p.}}\sqrt{\Lambda_{IJ}\omega_I\omega_J}/L, \tag{5}$$

where Λ_{IJ} is an overlap factor of spatial profiles of three participating modes, defined as

$$\Lambda_{IJ} = \left[(L/V)\int d\vec{r}_\perp u_z(\vec{r}_\perp) f_I(\vec{r}_\perp) f_J(\vec{r}_\perp)\right]^2, \tag{6}$$

with $I,\ J = 0,\ S$.

To complete the picture we need to add a term responsible for coupling with the environment, $\mathcal{H}_{\text{ext}}$, that can be expressed in terms of mode decay rates, $\kappa_{0,S}$ and γ_m, and corresponding external input fields, $\alpha_{0,S}^{\text{in}}$ and β_{th}: $\mathcal{H}_{\text{ext}} = \sum_{J=0,S} i\hbar\sqrt{\kappa_J}[a_J^\dagger a_J^{\text{in}} + a_J(a_J^{\text{in}})^*] + i\hbar\sqrt{\gamma_m}[b_m^\dagger b_{\text{th}} + b_m b_{\text{th}}^*]$. Here $a_0^{\text{in}} = (A_p + \delta a_0^{\text{in}})e^{-i\omega_p t}$ includes external laser pumping amplitude $A_p = \sqrt{P_{\text{in}}/(\hbar\omega_p)}$ and zero-mean fluctuations a_0^{in}, while two other modes are driven by fluctuations only. We assume optical mode fluctuations to be in a vacuum state so that $\langle a_{0,S}^{\text{in}}(t)(a_{0,S}^{\text{in}}(t'))^\dagger\rangle = \delta(t-t')$, and the mechanical damping noise, b_{th}, corresponds to thermal white noise with correlation function $\langle b_{\text{th}}(t)b_{\text{th}}^\dagger(t')\rangle = 2\gamma_m N_{\text{th}}\delta(t-t')$, where $N_{\text{th}} = (e^{\hbar\Omega_m/(k_B T)} - 1)^{-1}$ is the average number of thermal phonons in the mechanical mode, with k_B as Boltzmann's constant and T as mode temperature (usually, room temperature, $T = 300$ K, is assumed).

B. Natural scales and variable renormalization

In this study, we are interested in classical large-amplitude dynamics of the system described by the above Hamiltonian, which means high occupation numbers for all participating modes. Therefore, we change from quantum units to more physically sensible ones within the frames of this problem. For optical modes, a steady-state amplitude of light in the fixed-length Fabry-Pérot cavity, $A_c = 2A_p/\sqrt{\kappa_0} = \sqrt{4P_{\text{in}}/(\hbar\omega_0\kappa_0)} \equiv \sqrt{\bar{n}_c}$, looks to be a natural scale. The mechanical mode can be scaled by a displacement amplitude b_0 necessary to shift the Stokes mode frequency by one-half linewidth, i.e., $G_{0S}b_0 = \kappa_S/2$. The latter is a natural nonlinearity scale of an optomechanical system that sets the applicability limit for the linearized model thereof.

Hereafter we will operate with scaled amplitudes defined as

$$\alpha_{0,S} = a_{0,S}/A_c, \qquad \beta_m = b_m/b_0 = 2G_{0S}b_m/\kappa_S. \tag{7}$$

A similar transformation has to be applied to noise terms.

III. TEMPORAL DYNAMICS OF PARAMETRIC INSTABILITY

A. Equations of motion

One can now write Heisenberg-Langevin equations for the system described by Hamiltonian (3) in the frame that rotates with each mode frequency. This means doing substitutions $a_{0,S}(t) \to a_{0,S}(t)e^{-i\omega_{0,S}t}$ and $b_m(t) \to b_m(t)e^{-i(\Omega_m+\Delta_m)t}$ (here we define frequency mismatch as $\Delta_m = \omega_0 - \omega_S - \Omega_m$); then, dropping all the terms oscillating with frequency Ω_m and faster, one obtains

$$\dot{a}_0 = -\frac{\kappa_0}{2}a_0 + iG_{0S}a_S b_m + \sqrt{\kappa_0}(A_p + a_0^{\text{in}}), \tag{8a}$$

$$\dot{a}_S = -\left(\frac{\kappa_S}{2} + i\Delta_m\right)a_S + iG_{0S}a_0 b_m^\dagger + \sqrt{\kappa_S}a_S^{\text{in}}, \tag{8b}$$

$$\dot{b}_m = -\frac{\gamma_m}{2}b_m + iG_{0S}a_0 a_S^\dagger + \sqrt{\gamma_m}b_{\text{th}}. \tag{8c}$$

These equations can be rewritten in terms of dimensionless scaled amplitudes introduced in (7),

$$\dot{\alpha}_0 = -\frac{\kappa_0}{2}\alpha_0 + i\frac{\kappa_S}{2}\alpha_S\beta_m + \frac{\kappa_0}{2} + \sqrt{\kappa_0}\alpha_0^{\text{in}}, \tag{9a}$$

$$\dot{\alpha}_S = -\left(\frac{\kappa_S}{2} + i\Delta_m\right)\alpha_S + i\frac{\kappa_S}{2}\alpha_0\beta_m^\dagger + \sqrt{\kappa_S}\alpha_S^{\text{in}}, \tag{9b}$$

$$\dot{\beta}_m = -\frac{\gamma_m}{2}\beta_m + i\frac{\gamma_m}{2}\mathcal{R}_0\alpha_0\alpha_S^\dagger + \sqrt{\gamma_m}\beta_{\rm th}. \quad (9c)$$

Here we introduced an important quantity, a PI gain $\mathcal{R}_0 = 4G_{0S}^2\bar{n}_c/(\gamma_m\kappa_S)$, the significance of which will be revealed below. Note that amplitude β_m introduced by Eq. (7) practically coincides with dimensionless mechanical amplitude Z of [19].

As we are mostly interested in the strong signal dynamics of the three-mode system, the noise terms in the above equations may be safely omitted. However, a small initial nonzero amplitude of mechanical oscillations is necessary for a nontrivial solution. Brownian thermal vibrations of the mirror provide this initial amplitude of b_m, which is equal to $\sqrt{N_{\rm th}} \simeq (k_BT/(\hbar\Omega_m))^{1/2}$. Solving this system of equations numerically gives the characteristic result shown in Fig. 2.

B. Parametric instability criterion

For parametric instability to develop, a certain threshold of input pumping power has to be reached. Braginsky *et al.* [1] used the above-introduced PI gain, $\mathcal{R}_0$, as a figure of merit for PI in the resonance case of $\Delta_m = 0$ and defined it as

$$\mathcal{R}_0 = \frac{4G_{0S}^2\bar{n}_c}{\gamma_m\kappa_S} = \frac{8\Lambda_{0S}\omega_S P_{\rm in}}{m\Omega_m L^2\gamma_m\kappa_S\kappa_0} \equiv \frac{P_{\rm in}}{P_{\rm in}^{\rm thres}}, \quad (10)$$

where

$$P_{\rm in}^{\rm thres} = \frac{16G_{0S}^2}{\hbar\omega_0\kappa_0\kappa_S\gamma_m} = \frac{m\Omega_m L^2\gamma_m\kappa_S\kappa_0}{8\Lambda_{0S}\omega_S}$$

is the threshold input power value for resonant pumping.

If $\mathcal{R}_0 \geq 1$, the system becomes unstable; otherwise, no excitation of the mechanical and Stokes modes occurs. In a more general detuned case this criterion is only slightly modified,

$$\mathcal{R}_0 \geq 1 + \left(\frac{2\Delta_m}{\gamma_m + \kappa_S}\right)^2. \quad (11)$$

This condition as well as an instability onset time can be obtained using a simple linearized model based on Eqs. (9). To start, we assume the amplitude of a fundamental optical mode to be constant and equal to 1 in the normalization we choose. Then from Eqs. (9) we obtain the following set of linear equations for the Stokes and mechanical modes:

$$\dot{\alpha}_S^\dagger = -\left(\frac{\kappa_S}{2} - i\Delta_m\right)\alpha_S^\dagger - i\frac{\kappa_S}{2}\beta_m, \quad (12a)$$

$$\dot{\beta}_m = -\frac{\gamma_m}{2}\beta_m + i\frac{\gamma_m}{2}\mathcal{R}_0\alpha_S^\dagger. \quad (12b)$$

Looking for general solution in the form $\{\alpha_S^\dagger, \beta_m\} \propto e^{(\Gamma+i\nu)t}$, the PI condition, $\Gamma \geq 0$, is obtainable from the characteristic equation for the above linear system,

$$(\Gamma + i\nu + \kappa_S/2 - i\Delta_m)(\Gamma + i\nu + \gamma_m/2) - \gamma_m\kappa_S\mathcal{R}_0/4 = 0,$$

with the solution

$$\Gamma = \frac{1}{4}\left[\sqrt{X + \sqrt{X^2 + Y^2}} - (\kappa_S + \gamma_m)\right], \quad (13a)$$

$$\nu = \frac{\Delta_m}{2} - \frac{1}{4}\sqrt{\sqrt{X^2 + Y^2} - X}, \quad (13b)$$

where

$$X \equiv 2\gamma_m\kappa_S\mathcal{R}_0 - 2\Delta_m^2 + \frac{1}{2}(\kappa_S - \gamma_m)^2,$$

$$Y \equiv 2\Delta_m(\kappa_S - \gamma_m).$$

Requirement $\Gamma > 0$ yields the sought-for relations (10) and (11).

IV. ADIABATIC ELIMINATION OF CAVITY MODES

In gravitational-wave interferometers, as well as in small-scale, tabletop optomechanical experiments [22], the mechanical decay rate, γ_m, is much smaller than the decay rates of the optical degrees of freedom, $\kappa_{0,S} \gg \gamma_m$. Therefore one can safely assume that optical modes follow any changes in the mechanical mode almost instantaneously, without delay. Hence we can adiabatically eliminate optical modes by setting time derivatives in Eqs. (9a) and (9b) to zero and by expressing the two optical modes as functions of mechanical amplitude $\beta_m(t)$ as

$$\alpha_0(t) = \frac{1 + i\delta_m}{1 + i\delta_m + \frac{\kappa_S}{\kappa_0}|\beta_m(t)|^2}, \quad (14)$$

$$\alpha_S(t) = \frac{i\beta_m^\dagger(t)}{1 + i\delta_m + \frac{\kappa_S}{\kappa_0}|\beta_m(t)|^2}, \quad (15)$$

where we defined dimensionless detuning $\delta_m = 2\Delta_m/\kappa_S$. Substituting these expressions into Eq. (9c), one arrives at a single nonlinear differential equation for the mechanical amplitude β_m,

$$\dot{\beta}_m + \frac{\gamma_m}{2}\left(1 - \frac{\mathcal{R}_0(1 + i\delta_m)}{(1 + \frac{\kappa_S}{\kappa_0}|\beta_m|^2)^2 + \delta_m^2}\right)\beta_m = 0. \quad (16)$$

This equation displays the mechanism of saturation clearly. Indeed, the system becomes unstable when the real part of the expression in brackets turns negative, meaning a negative mechanical decay rate. However, the rise of

amplitude, β_m, entering the denominator renders the negative term smaller and smaller, eventually reaching the critical point when the bracket turns 0. From this ensues a new nonlinear parametric instability condition of the form

$$\mathcal{R}_{\mathrm{NL}} = \frac{\mathcal{R}_0}{(1+\frac{\kappa_S}{\kappa_0}|\beta_m|^2)^2 + (\frac{2\Delta_m}{\kappa_S})^2} \geq 1, \tag{17}$$

where the nonlinear gain, $\mathcal{R}_{\mathrm{NL}}$, gradually wanes as amplitude, β_m, waxes, reaching a limit cycle.

The value of the critical amplitude is identical to the steady-state amplitude, as $\beta_m(t)$ is a monotonic function of time and equals to

$$\bar{\beta}_m = \left[\frac{\kappa_0}{\kappa_S}\left(\sqrt{\mathcal{R}_0 - \delta_m^2} - 1\right)\right]^{1/2}. \tag{18}$$

Steady-state amplitudes for optical modes immediately ensue from Eqs. (15) and (14),

$$\bar{\alpha}_0 = \sqrt{\frac{1+\delta_m^2}{\mathcal{R}_0}}, \qquad \bar{\alpha}_S = \left[\frac{\kappa_0}{\kappa_S}\frac{1}{\mathcal{R}_0}\left(\sqrt{\mathcal{R}_0 - \delta_m^2} - 1\right)\right]^{1/2}. \tag{19}$$

An adiabatic limit can also help us to understand the small hump one can notice on the plot of the Stokes mode power in Fig. 2 for PI gain $\mathcal{R}_0 = 8$, which is absent on the other curves with lower gain. The existence of this hump stems from the dependence of the Stokes mode amplitude, α_S, on the mechanical amplitude, β_m, given by Eq. (15). If we consider the Stokes mode normalized power $|\alpha_S|^2$ and equate its time derivative to zero we get

$$\partial_t(|\beta_m|^2) \cdot \frac{1+\delta_m^2 - \frac{\kappa_S^2}{\kappa_0^2}|\beta_m|^2}{(1+\frac{\kappa_S}{\kappa_0}|\beta_m|^2)^2 + \delta_m^2} = 0,$$

which is a necessary condition for $|\alpha_S|^2$ to reach its extremum. As we know from the numerical solution, $\beta_m(t)$ is monotonic, and $\partial_t(|\beta_m|^2) = 0$ means that the mechanical amplitude has reached its maximal steady-state value $\bar{\beta}_m$. Therefore, the condition for the hump would be that the second term in the product above becomes equal to zero for $\beta_m < \bar{\beta}_m$, which, accounting for the monotonic character of $\beta_m(t)$, means that the numerator of the second term is smaller than zero at $\bar{\beta}_m$. From this immediately ensues a condition on parametric gain value above which one shall observe this hump in temporal behavior of the Stokes mode,

$$\mathcal{R}_0 > \left[\frac{\kappa_0}{\kappa_S}(2+\delta_m^2)\right]^2 + \delta_m^2 \underset{\delta_m=0,\kappa_0=\kappa_S}{\longrightarrow} 4. \tag{20}$$

Remarkably, in the resonance case ($\Omega_m = 0$), the value of PI gain above $\mathcal{R}_0 = 4$ that is the critical value for the hump development, corresponds to the situation when the power circulating in the Stokes mode becomes equal to the threshold value, i.e., to the power circulating in the fundamental optical mode. The hump represents the transient process of the initial excess growth of the Stokes mode occupation number above the threshold value, before the acoustic mode could reach its steady-state occupation number (recall that $\kappa_S \gg \gamma_m$) and further release this level through inverse scattering to the carrier mode. The latter process invokes recombination of the excess ω_S photons with acoustic phonons at Ω_m, yielding the generation of ω_0 photons. As shown by the greyed-out region in Fig. 2, when $\mathcal{R}_0 = 8$, the decrease of the fundamental mode power and the growth of the acoustic mode amplitude near the time when the Stokes mode maximum is reached becomes slower, which is indicative of the intensification of inverse scattering.

A. Approximate solution

By representing a complex function $\beta_m(t)$ as $|\beta_m(t)|e^{i\phi_m(t)}$ one can easily obtain the equations they satisfy from (16),

$$|\dot{\beta}_m| = -\frac{\gamma_m}{2}|\beta_m|\left(1 - \frac{\mathcal{R}_0}{(1+\frac{\kappa_S}{\kappa_0}|\beta_m|^2)^2 + \delta_m^2}\right), \tag{21a}$$

$$\dot{\phi}_m = -\frac{\gamma_m}{2}\frac{\delta_m \mathcal{R}_0}{(1+\frac{\kappa_S}{\kappa_0}|\beta_m|^2)^2 + \delta_m^2}. \tag{21b}$$

One can solve this system of first-order differential equations explicitly, but the result will be an implicit transcendental equation on β_m that cannot be resolved analytically. Nevertheless, a pretty good approximation thereof gives the solution of a simplified equation for β_m, obtainable by expanding the bracket in the r.h.s. of Eq. (21a) in $|\beta_m|$ around the $\bar{\beta}_m$ of Eq. (18). This results in a Bernoulli equation [32] of the shape

$$|\dot{\beta}_m| = \mathcal{D}|\beta_m|\left(1 - \frac{|\beta_m|}{\bar{\beta}_m}\right), \qquad \mathcal{D} = \frac{2\gamma_m \kappa_S \bar{\beta}_m^2}{\kappa_0 \mathcal{R}_0}\left(1 + \frac{\kappa_S}{\kappa_0}\bar{\beta}_m^2\right),$$

that, accounting for initial condition $|\beta_m(0)|$, resolves in

$$|\beta_m(t)| = \frac{|\beta_m(0)|\bar{\beta}_m e^{\mathcal{D}t}}{\bar{\beta}_m + |\beta_m(0)|(e^{\mathcal{D}t} - 1)}. \tag{22}$$

V. POWER RELATIONS IN THE THREE-MODE SYSTEM

It is obvious that in the adiabatic limit ($\Omega_m \ll \omega_{0,S}$), a sum of optical powers leaving the interferometer in the fundamental and the Stokes modes, i.e., $P_0^{\mathrm{out}} + P_S^{\mathrm{out}}$, must

be equal to the power $P_{\rm in}$ entering it. Power scattered in the acoustic mode is negligible compared to that of the optical modes due to a huge frequency difference. In order to see that it is indeed the case for our treatment one needs to write down standard input-output relations connecting light amplitudes outside the interferometer (of incident and reflected beams) with the intracavity ones derived in expressions (14) and (15),

$$a_0^{\rm in} + a_0^{\rm out} = \sqrt{\kappa_0} a_0 \Rightarrow A_p + A_0^{\rm out} = \sqrt{\kappa_0} A_0, \quad (23)$$

$$a_S^{\rm in} + a_S^{\rm out} = \sqrt{\kappa_S} a_S \Rightarrow A_S^{\rm out} = \sqrt{\kappa_S} A_S, \quad (24)$$

where capital letters identify classical components of the light fields we concerned with in this work. Powers in the corresponding beams are related to these amplitudes as $P_J = \hbar\omega_J |A_J|^2$ (J stands for p, 0, S). Assuming steady state, i.e., setting $\beta_m(t) \to \bar{\beta}_m$ in expressions (14) and (15), and normalization relations (7), one obtains expressions for the reflected light powers as follows:

$$P_0^{\rm out} = P_{\rm in} \frac{(1 - \frac{\kappa_S}{\kappa_0}|\bar{\beta}_m|^2)^2 + \delta_m^2}{(1 + \frac{\kappa_S}{\kappa_0}|\bar{\beta}_m|^2)^2 + \delta_m^2},$$

$$P_S^{\rm out} = P_{\rm in} \frac{4\frac{\kappa_S}{\kappa_0}|\bar{\beta}_m|^2}{(1 + \frac{\kappa_S}{\kappa_0}|\bar{\beta}_m|^2)^2 + \delta_m^2}.$$

There is no problem to see now that $P_0^{\rm out} + P_S^{\rm out} = P_{\rm in}$ and that the power balance is observed for any value of the acoustic mode amplitude $\bar{\beta}_m$. Substituting Eq. (18) in these equations, one gets the nonlinear input-output relations for the three-mode system above the PI threshold,

$$P_0^{\rm out} = P_{\rm in}\left[1\text{–}4\frac{\sqrt{\mathcal{R}_0 - \delta_m^2} - 1}{\mathcal{R}_0}\right], \quad (25)$$

$$P_0^{\rm out} = 4P_{\rm in}\frac{\sqrt{\mathcal{R}_0 - \delta_m^2} - 1}{\mathcal{R}_0}, \qquad \mathcal{R}_0 = \frac{P_{\rm in}}{P_{\rm in}^{\rm thr}}. \quad (26)$$

The dependence of outgoing power for each mode on PI gain and, therefore, on input power is drawn in Fig. 4.

The interesting feature of these relations is their apparent nonlinearity, which is quite opposite to a naive assumption one might be tempted to make that intracavity circulating power in both optical modes is linearly proportional to the outgoing power. Note, also, the existence of a critical value of input power corresponding to a PI gain of $\mathcal{R}_0 = 4$ (in the resonance case) when the reflected power in the carrier mode vanishes and the Stokes mode output reaches its maximum. The physics of this process is straightforward, for it is this level of power when the loss of carrier photons, due to three-mode scattering (into the Stokes and acoustic modes), reaches the level of the cavity bare loss, summarized in κ_0. This is a well-known phenomenon of critical coupling. This, in particular, has profound observational consequences, as measuring the PI by recording the beat note of the reflected lights at the carrier and Stokes mode frequencies may result in zero signal for the range of PI gains around the critical one, i.e., around $\mathcal{R}_0 \simeq 4$.

Returning to intracavity fields and recalling the definition of normalized modes (7), one can rewrite expressions (18) and (19) in more physical terms as

$$\frac{P_0}{\omega_0} = \frac{P_0^{\rm thr}}{\omega_0}\left[1 + \frac{4\Delta_m^2}{\kappa_S^2}\right], \quad (27)$$

$$\frac{P_S}{\omega_S} = \frac{P_0^{\rm thr}}{\omega_0}\left[\sqrt{\frac{P_{\rm in}}{P_{\rm in}^{\rm thr}} - \frac{4\Delta_m^2}{\kappa_S^2}} - 1\right], \quad (28)$$

$$\frac{P_m}{\Omega_m} = \frac{P_0^{\rm thr}}{\omega_0}\left[\sqrt{\frac{P_{\rm in}}{P_{\rm in}^{\rm thr}} - \frac{4\Delta_m^2}{\kappa_S^2}} - 1\right], \quad (29)$$

where

$$P_0^{\rm thr} = \hbar\omega_0 \frac{\gamma_m \kappa_0 \kappa_S}{4G_{0S}^2} = \frac{m\Omega_m L^2 \gamma_m \kappa_0 \kappa_S}{2\Lambda_{0S}\omega_S} \quad (30)$$

is the power circulating in the fundamental mode at resonance frequency ω_0 when the PI threshold is reached. The plots of these expressions are shown in Fig. 3. Here mechanical amplitude is inferred from the acoustic power, using its relation to acoustic amplitude, $P_m = \gamma_m \bar{\mathcal{H}}_m = \gamma_m m \Omega_m^2 \overline{x_m^2}$, yielding

$$\overline{x_m^2} = \frac{L^2 \kappa_0 \kappa_S}{2\Lambda_{0S}\omega_0\omega_S}\left[\sqrt{\frac{P_{\rm in}}{P_{\rm in}^{\rm thr}} - \frac{4\Delta_m^2}{\kappa_S^2}} - 1\right]. \quad (31)$$

Equations (28) and (29) have another interesting implication; namely, the equality

$$\frac{P_S}{\omega_S} = \frac{P_m}{\Omega_m} \quad (32)$$

represents the well-known Manley-Rowe relations for nonlinear interacting systems [33–35]. In our case, this equality means that the number of Stokes photons produced from the ω_0 photons matches exactly the number of acoustic phonons generated in this process.

One might wonder if there is an inverse process going on in the system, i.e., the generation of ω_0 photons from the pairs of ω_S photons and Ω_m phonons, and if this process would prevent the power circulating in the Stokes mode to exceed that in the fundamental mode. Indeed, such inverse scattering may happen and, were it not for constant pumping of laser photons into the system at frequency ω_0, there would be equal probability for direct and inverse

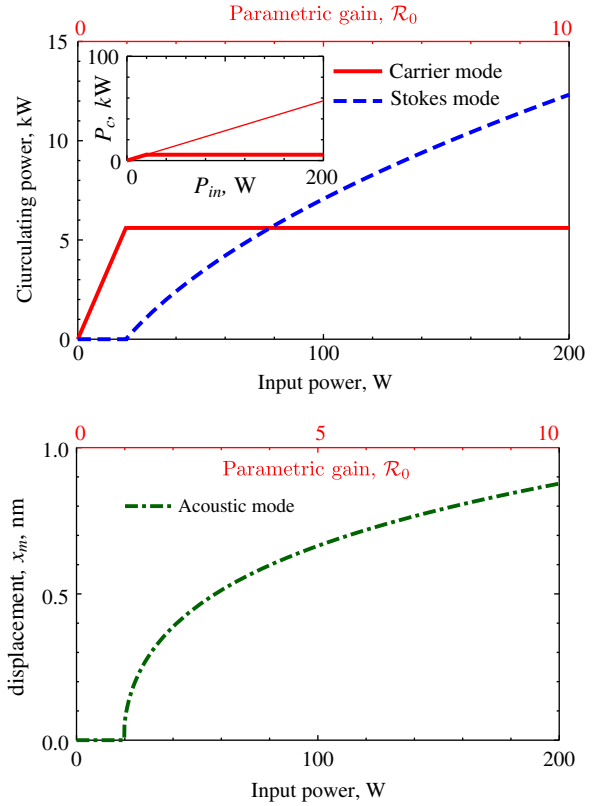

FIG. 3 (color online). Upper panel: Dependence of power circulating in the fundamental mode (red solid line) and in the higher-order Stokes mode (blue dashed line) on input power, calculated from Eqs. (27)–(29), using parameters from Table I. Inset plot compares the behavior of circulating power with (thick red line) and without (thin red line) PI. Lower panel: Dependence of acoustic mode amplitude on input laser power for parameters listed in Table I.

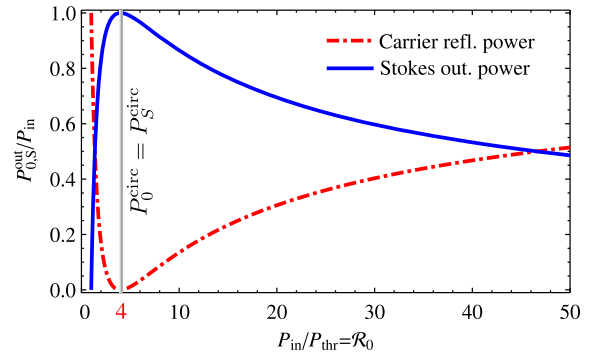

FIG. 4 (color online). Dependence of reflected light power at the carrier frequency ω_0 (red dash-dotted line) and at the HOM frequency (blue line) as a function of parametric gain $\mathcal{R}_0$ and, therefore, of input power. Note the nonlinear and nonmonotonic relation between the input and reflected powers. The critical PI gain value of $\mathcal{R}_0 = 4$ corresponds to the case of critical coupling, i.e., when the nonlinear loss of carrier photons to the Stokes mode and the acoustic mode reaches the level of bare loss of the interferometer defined by the reflectivities of the mirrors.

scattering processes, leading to equilibrium between the occupation numbers of the modes. One has to remember about losses that constantly drain photons and phonons from the corresponding modes; it is these losses to which the PI threshold (10) owes its existence.

The threshold of PI represents the level of intracavity power at which no more ω_0 photons can be born by the fundamental mode. Let the power in the Stokes mode reach a level slightly higher than the threshold power, as represented by the crossing of blue and red lines in the upper panel of Fig. 3. This means that input power is more than 4 times higher than $P_{\rm in}^{\rm thr}$. The inverse scattering process creates then a photon at ω_0, thereby making the fundamental mode have one photon more than the threshold allows. This photon cannot decay away using the fundamental mode loss channel, as it is saturated at the 4-times-lower input power level of $P_{\rm in}^{\rm thr}$. The only way for it to escape is through scattering again to the Stokes photon and the acoustic phonon. The probability of this scattering is higher than that of escaping the cavity because the optoacoustic photon-phonon exchange rate $G_{0S}\bar{n}_c^{1/2}$ is faster than the cavity decay rate κ_0, which is the prerequisite for parametric instability to start in the first place.

VI. TIME SCALE OF INSTABILITY: ONSET TIME

Using expression (13a) for Γ, one can derive a time scale for the instability onset, which is a time scale at which the linearized model breaks down and exponential ring-up gives place to a saturation and, eventually, to a new equilibrium state reached by a system. It can be estimated as a moment when the exponentially growing mechanical amplitude, $\beta_m(t) \simeq \beta_m(0)e^{\Gamma t}$, with $\beta_m(0) = \sqrt{4G_{0S}^2 N_{\rm th}/\kappa_S^2}$, reaches the above-calculated steady-state level, $\bar{\beta}_m$ of Eq. (18), i.e.,

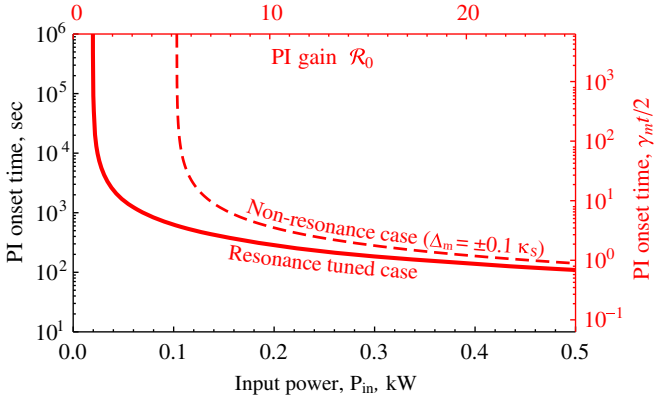

FIG. 5 (color online). Characteristic time for nonlinearity in parametric instability to take over. Thin dashed line shows the effect of nonzero frequency mismatch ($\Delta_m = \pm 0.1\kappa_S$ for this plot).

TABLE I. Parameters used for simulation.

Parameter	Notation	Value
Effective mass, kg	m	40
Arm length, km	L	4
Overlap factor	Λ	1.0
Fundamental mode finesse	$\mathcal{F}_0$	450
Stokes mode finesse	$\mathcal{F}_S$	450
Acoustic frequency, kHz	$\Omega_m/2\pi$	20
Acoustic mode Q	Q_m	10^7
Temperature, K	T	300
PI gain	$\mathcal{R}_0$	$0.05(\frac{P_{\rm in}}{1\ \rm W})$

$$|\beta_m(0)|e^{\Gamma\tau_{\rm PI}}=\bar{\beta}_m \Rightarrow$$
$$\tau_{\rm PI}=\frac{1}{2\Gamma}\log\frac{\kappa_0\kappa_S(\sqrt{\mathcal{R}_0-\delta_m^2}-1)}{4G_{0S}^2N_{\rm th}}$$
$$=\frac{1}{2\Gamma}\log\frac{m\Omega_m^2L^2\kappa_0\kappa_S(\sqrt{\mathcal{R}_0-(2\Delta_m/\kappa_S)^2}-1)}{2\Lambda_{0S}\omega_0\omega_S k_BT}. \quad (33)$$

This expression can be simplified if we recall that in real interferometers $\gamma_m \ll \kappa_S$ and condition $\Delta_m \ll \kappa_S$ should be satisfied for PI to arise. Expanding Eq. (13a) in a Taylor series in γ/κ and Δ_m/κ_S, one obtains

$$\Gamma \simeq \frac{\gamma_m\mathcal{R}_0}{2}[1-\mathcal{R}_0^{-1}-\delta_m^2].$$

Thus one can get the following approximate expression for PI onset time:

$$\tau_{\rm PI}\simeq\frac{1-\mathcal{R}_0^{-1}+\delta_m^2}{\gamma_m\mathcal{R}_0}\log\frac{\bar{n}_c\kappa_0}{\bar{N}_{th}\gamma_m}\frac{(\sqrt{\mathcal{R}_0-\delta_m^2}-1)}{\mathcal{R}_0}$$
$$=\frac{1-\mathcal{R}_0^{-1}+\delta_m^2}{\gamma_m\mathcal{R}_0}\log\frac{4P_{\rm in}\Omega_m}{k_BT\omega_0\gamma_m}\frac{(\sqrt{\mathcal{R}_0-\delta_m^2}-1)}{\mathcal{R}_0}. \quad (34)$$

The dependence of PI onset time versus pump laser power $P_{\rm in}$ (and PI gain) is plotted in Fig. 5 for parameters characteristic of the Advanced LIGO detector, which are given in Table I.

VII. DUAL-RECYCLING INTERFEROMETER

The above results are obtained for a single Fabry-Pérot cavity. However, they are easily generalized to the case of a power- and signal-recycled interferometer like the one of Advanced LIGO. Such an interferometer, if perfectly symmetric, is equivalent to two effective Fabry-Pérot interferometers with effective linewidths, $\kappa_{0\pm}$, and detunings, $\delta_\pm$, defined in terms of arm cavity parameters and power- and signal-recycling mirror (PRM and SRM) reflectivity and phase shift. Graphically, this fact is illustrated in Fig. 6. This result is well known as the "scaling law" and was devised by Buonanno and Chen in their seminal article [36].

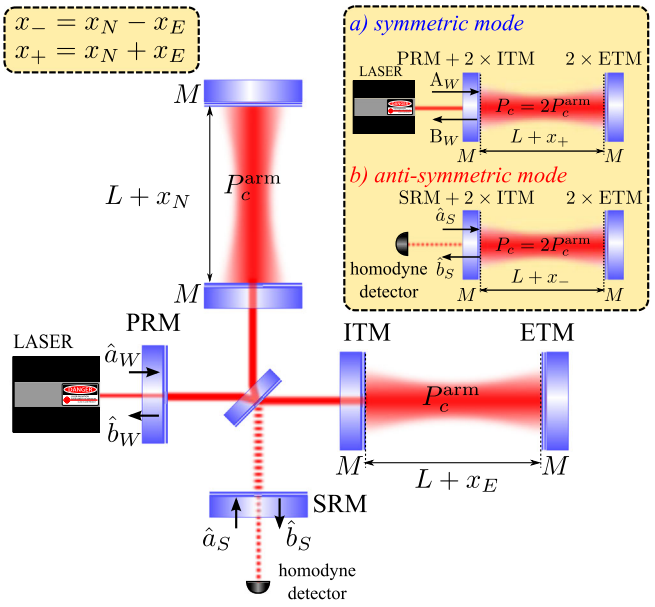

FIG. 6 (color online). Scaling law for dual-recycled Advanced LIGO interferometers: Common and differential modes of a balanced interferometer, representing the sum and difference of the optical fields in the arm cavities, can be modeled as two independent effective Fabry-Pérot cavities coupled to common and differential acoustic modes of the arm cavity mirrors.

The effective Fabry-Pérot cavities represent so-called symmetric and antisymmetric optical modes, which are coupled to corresponding common and differential acoustic modes of the mirrors (see related definitions in Sec. 5.3 of [37]). As shown in [9], the above consideration of three-mode parametric instability in Fabry-Pérot applies to each of these modes with the following substitutions of parameters:

$$M \to M, \quad (35)$$
$$P_c \to 2P_c^{\rm arm}, \quad (36)$$
$$\kappa_0 \to \kappa_{0\pm} = \kappa_0\Re\left[\frac{1-\rho_{p,s}e^{2i\phi_{p,s}^0}}{1+\rho_{p,s}e^{2i\phi_{p,s}^0}}\right], \quad (37)$$
$$\kappa_S \to \kappa_{S\pm} = \kappa_S\Re\left[\frac{1-\rho_{p,s}e^{2i\phi_{p,s}^S}}{1+\rho_{p,s}^Se^{2i\phi_{p,s}}}\right], \quad (38)$$
$$\Delta_m \to \Delta_m+\delta_\pm = \Delta_m+\kappa_0\Im\left[\frac{1-\rho_{p,s}e^{2i\phi_{p,s}}}{1+\rho_{p,s}e^{2i\phi_{p,s}}}\right], \quad (39)$$

where $\rho_{p,s}=\sqrt{1-T_{p,s}}$ are (amplitude) reflectivities of power- and signal-recycling mirrors, respectively, with $T_{p,s}$ being the more habitual power transmissivities thereof, and $\phi_{p,s}^{0,S}=\omega_{0,S}l_{p,s}/c$ are propagation phase shifts that light of

frequency $\omega_{0,S}$ acquires propagating the distance $l_{p,s}$ from arm cavity input test masses to the PRM and SRM, respectively. Here "+" sign stands for values that refer to a symmetric mode, and "−" sign indicates those of an antisymmetric one.

One can notice that the new linewidth ratio $\kappa_{0\pm}/\kappa_{S\pm}$ may be different from the one for the simple Fabry-Pérot, as phase shifts $\phi^0_{p,r}$ deviate from $\phi^S_{p,r}$; i.e., the fact that the fundamental mode is resonant in the power-recycled (PR) or signal-recycled (SR) cavity does not mean that the same is true for the Stokes mode. The difference is $\Delta\phi = \phi^0_{p,r} - \phi^S_{p,r} \simeq \Omega_m l_{p,r}/c$, which might be significant for the ∼25-m-long PR/SR cavities planned for Advanced LIGO.

Asymmetry in interferometer arms does not change the general conclusion of this section, for the dual-recycled interferometer can still be represented as two independent Fabry-Pérot interferometers, as shown in [14,38]. In this case, however, normal modes of the asymmetric system are not pure symmetric and antisymmetric combinations of fields in the arm cavities, but a general linear combination thereof (cf. Section 2.6 of [38]).

VIII. CONCLUSION

In this work, we analyzed, using full nonlinear treatment, the dynamics of three-mode optomechanical instability in large-scale gravitational-wave interferometers with freely suspended optics. It turns out that intrinsic nonlinearity of the three-mode interaction does not allow excited unstable optical and acoustic mode amplitudes to grow unbounded; rather, it makes them saturate to the new steady-state values. These values are governed by three dimensionless parameters: Parametric gain, $\mathcal{R}_0$, normalized frequency mismatch (detuning), $\delta_m = 2(\omega_0 - \omega_S - \Omega_m)/\kappa_S$, and the ratio of optical linewidths κ_0/κ_S. Therefore, our theory can be equally applied to simple Fabry-Pérot interferometers and to complex dual-recycled interferometers of the second-generation gravitational-wave detectors, such as Advanced LIGO [6,7], Advanced Virgo [10], KAGRA [11], and GEO-HF [12].

Our analysis shows that the process of instability development is quite slow for large-scale detectors, lasting for many relaxation times of the acoustic modes, which, due to very high Q factors of these modes, amounts to hundreds to thousands of seconds. Such a long onset time allows for efficient control and mitigation of this type of instability. Moreover, for reasonable values of PI gain, $\mathcal{R}_0 \sim 10$, consistent with recent parametric instability modeling for Advanced LIGO interferometers [4,5], acoustic mode amplitudes should not exceed nanometer level. Based on this point, as well as on the fact that the small-scale membrane-in-the-middle interferometer in UWA (where PI was observed experimentally in the nonlinear regime [22]) did not lose lock, one can presume that the same would be the case for a large-scale GW detector. However, there remains a high level of uncertainty pertaining to a greater complexity of an electronic control of a large interferometer. The response of the electronic control system to a slump of circulating power in the arms when PI starts to develop deserves a separate study.

It should be also noted that our theory assumes fixed, time-independent values of mode frequencies and optomechanical coupling. In real interferometers with suspended optics, mirrors tend to move around slowly and a laser beam spot does not rest at a fixed position on a mirror surface. This results in slow (compared to acoustic frequencies) modulation of the frequencies of the Stokes modes and therefore of the mismatch parameter, $\Delta_m(t)$, the PI gain $\mathcal{R}_0(t)$, and the modes' overlap factor Λ; this leads to reduced chance of instability. The effect of such modulation will be reported elsewhere [39].

ACKNOWLEDGMENTS

The authors are grateful to Andrey Matsko, Haixing Miao, and Huan Yang for fruitful and elucidating discussions, as well as to all the members of the Macroscopic Quantum Mechanics discussion group for helpful comments and suggestions on improvement of our manuscript. We also thank anonymous referees for constructive critics and useful comments that, we hope, helped refine the presentation and quality of our manuscript substantially. The work of D. G. B., J. L., and C. Z. is supported by the Australian Research Council. S. P. V. is supported by Russian Foundation for Basic Research (Grants No. 14-02-00399A and No. 13-02-92441) and by the National Science Foundation (Grant No. PHY-130586). S. D. is grateful to the University of Western Australia for support under the UWA Postdoctoral Research Fellowship scheme.

[1] V. B. Braginsky, S. E. Strigin, and S. P. Vyatchanin, Phys. Lett. A **287**, 331 (2001).
[2] S. P. Vyatchanin and S. E. Strigin, Phys. Usp. **55**, 1115 (2012).
[3] S. Strigin and S. Vyatchanin, Phys. Lett. A **365**, 10 (2007).
[4] S. Gras, D. G. Blair, and C. Zhao, Classical Quantum Gravity **26**, 135012 (2009).
[5] M. Evans, L. Barsotti, and P. Fritschel, Phys. Lett. A **374**, 665 (2010).
[6] K. Thorne, The Scientific Case for Advanced Ligo Interferometers, LIGO document P000024-x0, (2001), https://dcc.ligo.org/P000024/public.

[7] P. Fritschel, in *Gravitational-Wave Detection*, edited by M. Cruise and P. Saulson, Proc. SPIE Vol. 4856 (SPIE, Bellingham, WA, 2003), p. 282.
[8] S. P. Vyatchanin and S. E. Strigin, Quantum Electron. **37**, 1097 (2007).
[9] A. Gurkovsky, S. Strigin, and S. Vyatchanin, Phys. Lett. A **362**, 91 (2007).
[10] F. Acernese *et al.*, J. Phys. Conf. Ser. **32**, 223 (2006).
[11] K. Somiya, Classical Quantum Gravity **29**, 124007 (2012).
[12] B. Willke *et al.*, Classical Quantum Gravity **23**, S207 (2006).
[13] C. Zhao, L. Ju, J. Degallaix, S. Gras, and D. G. Blair, Phys. Rev. Lett. **94**, 121102 (2005).
[14] S. Gras, C. Zhao, D. G. Blair, and L. Ju, Classical Quantum Gravity **27**, 205019 (2010).
[15] J. Degallaix, C. Zhao, L. Ju, and D. Blair, J. Opt. Soc. Am. B **24**, 1336 (2007).
[16] L. Ju, D. G. Blair, C. Zhao, S. Gras, Z. Zhang, P. Barriga, H. Miao, Y. Fan, and L. Merrill, Classical Quantum Gravity **26**, 015002 (2009).
[17] S. Gras, D. G. Blair, and C. Zhao, Classical Quantum Gravity **26**, 135012 (2009).
[18] J. Miller, M. Evans, L. Barsotti, P. Fritschel, M. MacInnis, R. Mittleman, B. Shapiro, J. Soto, and C. Torrie, Phys. Lett. A **375**, 788 (2011).
[19] A. G. Polyakov and S. P. Vyatchanin, Phys. Lett. A **368**, 423 (2007).
[20] A. B. Matsko, A. A. Savchenkov, V. S. Ilchenko, D. Seidel, and L. Maleki, Phys. Rev. Lett. **103**, 257403 (2009).
[21] A. B. Matsko, A. A. Savchenkov, and L. Maleki, Opt. Express **20**, 16234 (2012).
[22] X. Chen *et al.*, arXiv:1411.3016.
[23] H. Kogelnik and T. Li, Appl. Opt. **5**, 1550 (1966).
[24] W. Kells and E. D'Ambrosio, Phys. Lett. A **299**, 326 (2002).
[25] I. Wilson-Rae, P. Zoller, and A. Imamoglu, Phys. Rev. Lett. **92**, 075507 (2004).
[26] I. Wilson-Rae, N. Nooshi, J. Dobrindt, T. J. Kippenberg, and W. Zwerger, New J. Phys. **10**, 095007 (2008).
[27] A. Schliesser, P. Del'Haye, N. Nooshi, K. J. Vahala, and T. J. Kippenberg, Phys. Rev. Lett. **97**, 243905 (2006).
[28] T. Rocheleau, T. Ndukum, C. Macklin, J. B. Hertzberg, A. A. Clerk, and K. C. Schwab, Nature (London) **463**, 72 (2010).
[29] A. Schliesser, O. Arcizet, R. Riviere, G. Anetsberger, and T. J. Kippenberg, Nat. Phys. **5**, 509 (2009).
[30] A. Yariv and W. Louisell, IEEE J. Quantum Electron. **2**, 418 (1966).
[31] L. Ju, C. Zhao, Y. Ma, D. G. Blair, S. L. Danilishin, and S. Gras, Classical Quantum Gravity **31**, 145002 (2014).
[32] A. D. Polyanin and V. F. Zaitsev, *Handbook of Exact Solutions for Ordinary Differential Equations*, 2nd ed. (Chapman and Hall/CRC, Boca Raton, FL & New York, 2003).
[33] R. W. Boyd, *Nonlinear Optics*, 2nd ed. (Academic Press, New York, 2003).
[34] J. M. Manley and H. Rowe, Proc. IRE **44**, 904 (1956).
[35] H. Rowe, Proc. IRE **46**, 850 (1958).
[36] A. Buonanno and Y. Chen, Phys. Rev. D **67**, 062002 (2003).
[37] S. L. Danilishin and F. Y. Khalili, Living Rev. Relativity **15**, 5 (2012).
[38] S. Strigin and S. Vyatchanin, Phys. Lett. A **365**, 10 (2007).
[39] C. Zhao, L. Ju, Q. Fang, C. Blair, J. Qin, D. Blair, J. Degallaix, and H. Yamamoto, LIGO document P1400250-v1, (2014), https://dcc.ligo.org/DocDB/0116/P1400250/001/PIModu_20141128.pdf.